INTERNATIONAL JOURNAL OF HYDROGEN ENERGY 48 (2023) 19580–19595

Available online at www.sciencedirect.com

ScienceDirect

journal homepage: www.elsevier.com/locate/he

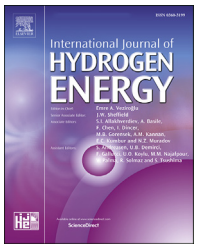

Membrane reactors for green hydrogen production from biogas and biomethane: A techno-economic assessment

Michele Ongis [a,b,*], *Gioele Di Marcoberardino* [c], *Giampaolo Manzolini* [a], *Fausto Gallucci* [b], *Marco Binotti* [a,**]

[a] *Politecnico di Milano, Dipartimento di Energia, via Lambruschini 4a, 20156, Milano, Italy*
[b] *Eindhoven University of Technology, Department of Chemical Engineering and Chemistry, Sustainable Process Engineering, De Rondom 70, Eindhoven 5612 AP, the Netherlands*
[c] *Università degli Studi di Brescia, Dipartimento di Ingegneria Meccanica e Industriale, via Branze 38, 25123, Brescia, Italy*

HIGHLIGHTS

- Small-scale hydrogen production process intensification with membrane reactors.
- Biogas and biomethane autothermal reforming are compared.
- Detailed model of the fluidized bed membrane reactor and of the overall process.
- Optimization of reactor and system performance and of levelized cost of hydrogen.

ARTICLE INFO

Article history:
Received 26 August 2022
Received in revised form
21 January 2023
Accepted 25 January 2023
Available online 1 March 2023

Keywords:
Hydrogen production
Biogas
Biomethane
Membrane reactors
Process intensification
Modelling

ABSTRACT

This work investigates the performance of a fluidized-bed membrane reactor for pure hydrogen production. A techno-economic assessment of a plant with the production capacity of 100 kg_{H2}/day was carried out, evaluating the optimum design of the system in terms of reactor size (diameter and number of membranes) and operating pressures. Starting from a biomass source, hydrogen production through autothermal reforming of two different feedstock, biogas and biomethane, is compared.

Results in terms of efficiency indicates that biomethane outperforms biogas as feedstock for the system, both from the reactor (97.4% vs 97.0%) and the overall system efficiency (63.7% vs 62.7%) point of views. Nevertheless, looking at the final LCOH, the additional cost of biomethane leads to a higher cost of the hydrogen produced (4.62 €/$kg_{H2@20\ bar}$ vs 4.39 €/$kg_{H2@20\ bar}$), indicating that at the current price biogas is the more convenient choice.

* *Corresponding author*. Politecnico di Milano, Dipartimento di Energia, via Lambruschini 4a, 20156, Milano, Italy.
** *Corresponding author*.
E-mail addresses: michele.ongis@polimi.it (M. Ongis), marco.binotti@polimi.it (M. Binotti).

https://doi.org/10.1016/j.ijhydene.2023.01.310

Nomenclature

A	Reactor cross section. $m^2_{reactor}$
C_i	Cost of plant component *i*. k€
$C_{i,0}$	Reference cost of plant component *i*. k€
$C_{i,b}$	Concentration of chemical component *i* in bubble phase kmol/$m^3_{reactor}$
$C_{i,e}$	Concentration of chemical component *i* in emulsion phase kmol/$m^3_{reactor}$
$CEPCI_y$	Chemical Engineering Plant Cost Index at year y
$d_{membrane}$	Diameter of a single membrane. $m_{membrane}$
$E_{a,j}$	Activation energy of reaction *j*. kJ/mol
$E_{a,perm}$	Activation energy term in permeance calculation. kJ/mol
$F_{H_2,perm}$	Total hydrogen permeated through membranes per unit length. kmol/(h·$m_{reactor}$)
F_i	Molar flow rate of component *i* along the reactor kmol/h
h_{eq}	Equivalent hours of the plant. h/y
$J_{H_2,perm}$	Hydrogen permeated per unit of membrane area kmol/(h·$m_{membrane}$· $m_{reactor}$)
K_{be}	Exchange coefficient between bubble and emulsion phase. 1/h
$K_{eq,j}$	Equilibrium constant of reaction *j*. bar^x
k^0_j	Pre-exponential factor of reaction *j*. kmol/(h·kg_{cat}·bar^x)
m_F	Total mass of fuel (BM or BG) fed to the system. kg/s
m_{H_2}	Total mass of pure hydrogen produced. kg/s
n	Exponential parameter in Richardson's law. -
$n_{CH_4,in}$	Moles of methane fed to the membrane reactor kmol/h
n_{H_2}	Total moles of pure hydrogen produced. kmol/h
$N_{membranes}$	Number of membranes inserted in the membrane reactor.
$n_{O_2,in}$	Moles of oxygen fed to the membrane reactor kmol/h
NR	Number of chemical reactions involved
p	Pressure. bar
$Per^0_{H_2}$	Permeance pre-exponential factor of hydrogen through the membrane. kmol/(h·$m_{membrane}$·$m_{reactor}$ ·bar^n)
p_i	Partial pressure of component *i*. bar
R	Universal gas constant. kJ/(mol·K)
r_j	Reaction rate of reaction *j*. kmol/(h·kg_{cat})
S_i	Size of component *i*. kg or m^2 or kW or L/h
$S_{i,0}$	Reference size of component *i*. kg or m^2 or kW or L/h
T	Reactor temperature. K
u	Superficial velocity of the gas crossing the reactor. $m_{reactor}$/s
u_{mf}	Gas velocity to maintain the bed in minimum fluidization conditions. $m_{reactor}$/s
W_{aux}	Auxiliaries consumption. kW
z	Axial position along the reactor. $m_{reactor}$

Greek Letters

δ_b	Bubble-phase fraction.
ΔT	Temperature difference. K
$\eta_{el,ref}$	Average electric efficiency of the power generating park. %
$\nu_{j,i}$	Stoichiometric coefficient of component *i* in reaction *j*. -
ρ_{cat}	Apparent density of catalyst particles packed in the reactor kg/$m^3_{reactor}$

Acronyms

ACM	Aspen Custom Modeler®
AP	Aspen Plus®
BG	BioGas
BM	BioMethane
CCF	Capital Charge Factor
CFD	Computational Fluid Dynamics
C&OC	Owner's and contingencies costs
FBMR	Fluidized Bed Membrane Reactor
GHGs	GreenHouse Gases
HRF	Hydrogen Recovery Factor
IC	Indirect costs
IEA	International Energy Agency
LCOH	Levelized Cost Of Hydrogen, €/kg
LHV	Lower Heating Value, kJ/kg
MR	Membrane Reactor
O&M	Operation and Maintenance costs, €
SEC	Specific Energy Consumption, kWh/kg
TIC	Installation costs
TPC	Total Plant Cost, k€
TRL	Technology Readiness Level

Introduction

Decarbonization of the energy sector plays a fundamental role in the reduction of greenhouse gases (GHGs) emissions. Many results have been achieved in recent years for clean electricity production by low-carbon sources and the total share of electricity in global final energy consumption is growing. Net Zero by 2050 scenario of the International Energy Agency (IEA) claims a share of almost 50% electricity on total energy consumption in 2050 [1]. In the stated policies scenario, reported again by IEA [2], the share of electricity goes from 19% in 2018 to 24% in 2040. Despite this improvement, these numbers indicate that the transition of the electric sector only cannot be enough on its own in the overall GHGs emission reduction, particularly since global energy demand is constantly growing. In the stated policies scenario, world energy demand for 2040 is expected to increase by 50% compared to the value in 2019 [2]. Since electrification only cannot bear the entire burden of decarbonization, multiple fuels and technologies will be needed in this process. Among them, a critical role in the hard-to-abate sectors, such as heating and mobility, is played by low-carbon gaseous carriers, led by biogas, biomethane and low-carbon hydrogen. The potential diffusion of

hydrogen-based systems, such as fuel cell and industrial boilers, will result in a higher green H_2 demand.

Today, dedicated hydrogen production is about 72 million tonnes (Mt) every year. It is almost entirely produced by fossil fuels, mainly from steam methane reforming process, and implicates significant GHGs emissions, around 830 Mt of CO_2 every year [3]. To produce low-carbon hydrogen, the primary route is the usage of fossil fuels with carbon capture, utilization and storage, accounting for 0.9% of hydrogen production in 2020, followed by water electrolysis [4]. Another method to produce hydrogen from renewables sources is the usage of biomass, mainly through pyrolysis and gasification [5]. Emerging technologies for hydrogen production from biomass involves membrane technology, starting from biogas (BG) or biomethane (BM) obtained through biomass anaerobic digestion. Promising results for a single-step production, suitable particularly for distributed applications, have been recently obtained both with active proton-conductive ceramic membranes in proton ceramic reactors [6] and with Palladium-alloys based (Pd-based) membranes in membrane reactors [7]. In this work, the pathway investigated is green hydrogen production through steam methane reforming of BG or BM in membrane reactors containing Pd-based membranes.

Biogas is basically a mixture of methane and carbon dioxide, with traces of other gases (O_2, N_2, H_2, H_2O, H_2S, NH_3). It is mainly produced by anaerobic digestion in biodigesters, but can also be originated from landfill gas recovery systems or wastewater treatment plants. Biomethane is the renewable form of the natural gas, mainly composed by methane. About 90% of biomethane is produced from raw biogas, through a post-treatment process called *biogas upgrading*, while the remaining part is directly produced from solid biomass gasification followed by methanation [8]. In upgrading processes, carbon dioxide and other contaminants are removed from biogas, obtaining nearly pure methane (>98%) [9]. Mostly used processes for the upgrading are water scrubbing, chemical scrubbing, pressure swing adsorption and membrane technology. The choice of a particular process depends on many factors, such as the methane loss (from 0.04% to 4%), biogas pre-cleaning requirement, difficulties in control of the process, heat requirement, purity of produced biomethane and investment and operational costs. In Europe, most of the biogas is used for power generation, heat in buildings and cogeneration units, while only about 10% is upgraded to biomethane [8]. Nevertheless, it is progressively observed a shift towards upgrading, mainly due to advancement in upgrading technology, subsidies and new opportunities for biomethane in natural-gas powered vehicles and for its injection in the natural-gas grid [10]. Biogas production expected potential for 2040 is 50% larger than today [8]. Moreover, its production average cost is expected to fall over time. Its increasing availability, lower production cost and increasing in upgraded share to biomethane share make these two feedstocks interesting for green hydrogen production.

Process intensification via membrane reactor (MR) technology has been proposed as a promising option to reduce costs and increase efficiency for small-scale hydrogen production. By integrating selective membranes in the reactive zone of the reactor, pure hydrogen is produced in a single equipment, thus avoiding the expensive downstream processes. This concept is illustrated in Fig. 1. Moreover, products removal in the reactive zone allows to push forward chemical

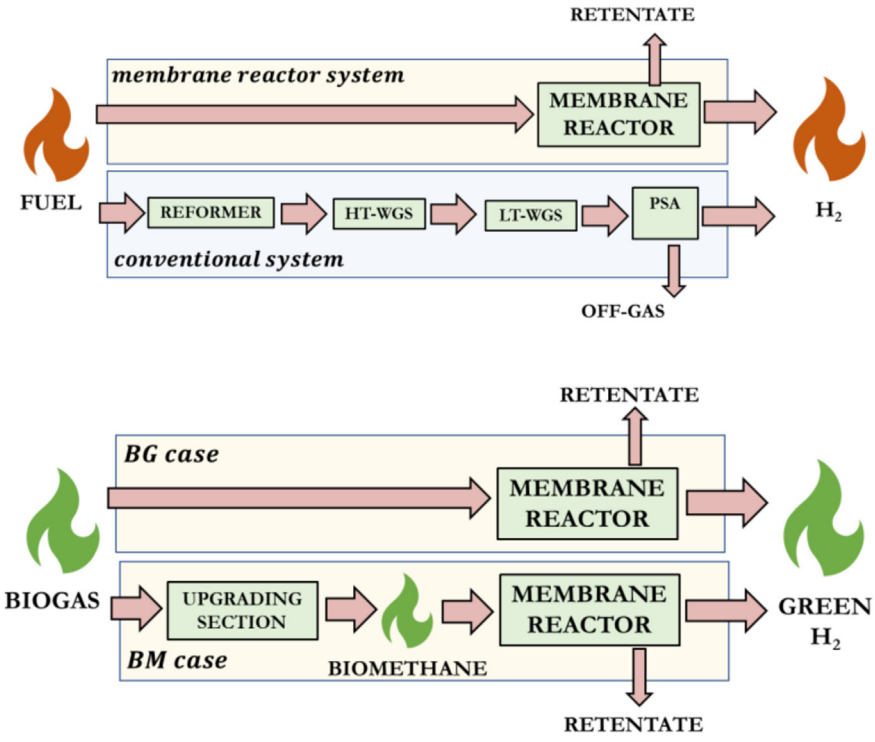

Fig. 1 – Top: concept of membrane reactor used for hydrogen production process intensification; Bottom: paths investigated in this work.

equilibrium limitations of reactions involved, leading to higher conversion compared to a conventional reformer reactor. MRs have shown interesting potentialities in different EU funded projects [11]. Particularly relevant for hydrogen production from biogas was BIONICO project [12], where a prototype of a Fluidized-Bed Membrane Reactor (FBMR) with the capacity of 100 kg/day was designed and built. Currently, the EU project MACBETH [13] aims to bring this technology to TRL7 by 2024 for different processes, including hydrogen production.

In this context, modelling activity is a fundamental support to the industrial development of MRs technology. This is particularly true in fluidized-bed configuration, where a complex fluid dynamics interacts with the reactive and the permeation process. A multi-scale modelling is in general necessary to have a precise description of the process. Permeation models [14] and kinetic models [15] have to be developed or selected from literature to be included in the FBMR model. At reactor level, detailed Computational Fluid Dynamics (CFD) and optical techniques can be used for a detailed description of some fundamentals about the fluidized bed behaviour [16–18]. The Reactor model should have a level of detail coherent with the aim of the analysis, being as much as possible consistent with the results of the fundamentals models. FBMR models in literature have been gradually developed to refine the phenomenological description [19–21]. At system level, reactor model is included in a broader process simulation to perform a techno-economic analysis of the overall system [22–25].

In this work, the use of a FBMR for pure hydrogen production through an autothermal reforming process is investigated. The size chosen is 100 kg/day, coherently with the prototypes developed within BIONICO and MACBETH, which represents a typical distributed hydrogen production plant for refuelling stations, glass industries and other small industries. In a previous work [23], the potentialities of the system had already been investigated by the identification of the maximum efficiency operating points together with a preliminary economic analysis using raw biogas as feedstock. Nevertheless, it was limited to the reactor diameters and membrane areas that led to the maximum system efficiency. Purpose of the present work is to perform a techno-economic assessment to compare biogas and biomethane as feedstocks for hydrogen production in a FBMR, based on the analysis performed in Ref. [23], with the following improvements: (i) the optimization is performed with an enhanced version of the model, showing clearly the efficiency trends obtained by varying the manipulated variables and (ii) the economic analysis is extended to all the working points investigated, since the economic optimum can in general be different from the technical optimum.

The use of biomethane, avoiding to feed carbon dioxide to the membrane reactor as in the biogas case, leads to higher partial pressure of the hydrogen in the reactor, thus increasing the driving force required for permeation. This in principle allows a reduction of the number of membranes required and of the reactor size, thus reducing the hydrogen production cost. On the other hand, biomethane production requires an upgrading section that can raise the total cost. Results are compared looking at reactor and system efficiencies and at the hydrogen cost.

General methodology is presented in section 2, together with the models assumptions and plant layout. The simulation results are presented in section 3. Section 4 describes the economic analysis, followed by conclusions in section 5.

Methodology

This work is based on a detailed mathematical model of the membrane reactor. The model has been realized in the software Aspen Custom Modeler® (ACM), which includes a database for the properties of the chemical components involved in the process and allows a direct integration with Aspen Plus® (AP), the software used to perform the simulation of the overall process.

In section 2.1, the general assumptions of the work will be listed, as well as the key performance indicators used to evaluate the performance from the point of views of both reactor and overall plant. The general methodology of the techno-economic assessment is mainly taken by Ref. [23], at which most of the assumptions refer to. In section 2.2 and 2.3, methodology of respectively the reactor model and the overall system model are presented.

General assumptions

Both ACM and AP allow to call various set of properties of the chemical components involved in the process. The equation of state selected for the computation of all the thermodynamic properties is the Peng-Robinson, widely used in processes involving hydrocarbons.

The feedstock of the process is biogas or biomethane depending on the case studied (BG case or BM case). BG composition is in general variable and depends on the biomass source: the one used in this work is taken from Ref. [23] and is reported in Table 1. BM composition, reported in Table 1, is taken from Ref. [26]. Lower Heating Values (LHVs) are provided by the software AP.

In the investigated cases, hydrogen is produced from biogas or biomethane reforming in an autothermal process. Considering all the chemical reactions involved, the chemical components present in the system are CH_4, H_2O, CO, CO_2, H_2, O_2, N_2. H_2S is not considered as membranes and reforming catalyst would not withstand the presence of H_2S [27] and thus this component needs to be separated before the reactor (as it happens in conventional reforming).

Reactor type and reactor model

The FBMR is a cylindrical vessel with the membranes vertically inserted from the top part of the reactor. In this work, the

Table 1 – Biogas and biomethane mole fractions (%) used in this work.

Species	Biogas	Biomethane
CH_4	58.1	96.0
CO_2	33.9	2.0
N_2	3.8	1.5
O_2	1.1	0.5
H_2O	3.1	–
LHV (MJ/kg)	17.8	45.7

membranes are composed by a selective Pd–Ag layer plated on a ceramic support, as described in Ref. [7], with a cylindrical structure and an inner cylindrical space for hydrogen collection where vacuum is obtained through a vacuum pump. Reactants (*feed*) are fed from the bottom of the reactor and flow towards the top. Hydrogen collected in the inner part of the membrane is called *permeate*, while the chemical components which flows towards the top without crossing the membranes compose the *retentate*. The gas flowing in the reactor should have enough superficial velocity to drag the catalyst particles, bringing the reactor in bubbling fluidization regime. From the modelling point of view, the reactor can be divided in three different regions: the bottom part, where only catalyst is present (no membranes), is a pure reactive region, as in a conventional fluidized bed reactor (this allows producing hydrogen and effectively using the membranes afterward); the central part, once membranes start, in which both chemical reactions and permeation occur; at the top of the reactor, above the membranes, there is the freeboard region where in general reactor section increases to slow down the retentate gas, allowing the solid catalyst particles to fall down again in the region where membranes operate. Reactor structure is represented in Fig. 2.

The model describes the first two sections: the reaction zone and the permeation zone, then assuming that the presence of catalyst particles in the freeboard region does not lead to an additional conversion. It is a 1D model, discretized along the vertical length of the reactor, here referred as direction z. The fluidized-bed is modelled according to the two phase theory: *bubble phase* and *emulsion-wake phase* [28]. Bubbles are spherical and their diameters - increasing with height - as well as the total amount of bubbles into the reactor, are evaluated from correlations obtained for a fluidized-bed reactor without membranes [29], since no accurate correlations for fluidized-bed with immersed membranes are available yet. The ACM code of the model, as well as its mathematical description, is based on a previous work [21], where a detailed description of the model as well as all the correlations used are reported,

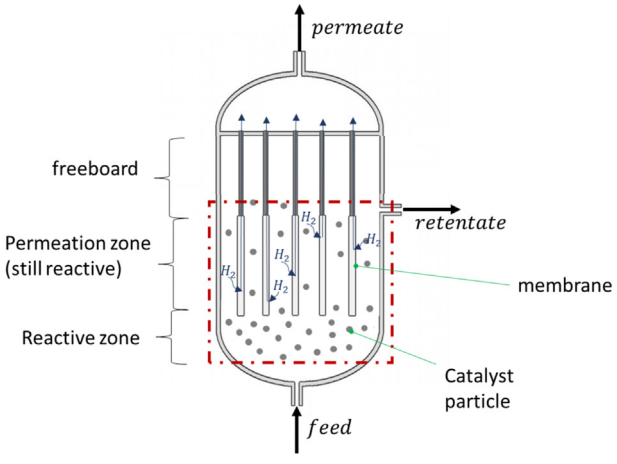

Fig. 2 – Schematic of the FBMR structure. In red, the sections considered in the model. (For interpretation of the references to color in this figure legend, the reader is referred to the Web version of this article.)

including calculations for minimum fluidization velocity, void fraction, bubble diameter, bubble and emulsion phase fractions, wake fraction and exchange coefficients between the phases. In this model it is assumed that no solid particles are present in the bubble phase, therefore no reactions occur inside them. The bottom part of the bubble is called wake and contains solid particles. Wake fraction is calculated starting from bubble fraction by a correlation taken from Ref. [17]. Emulsion phase is assumed to be in minimum fluidization conditions and is the phase where chemical reactions happen. For simplicity, also the wake is assumed to be in minimum fluidization condition. Accordingly, emulsion and wake phases can be considered as a unique emulsion-wake phase. The excess gas flows as bubbles inside the bed. Moreover, it is assumed that hydrogen permeation through the membranes occurs from both bubble and emulsion phases according to their fraction.

The model performs material balances in each element *dz* and an overall energy balance to verify the autothermal behaviour of the reactor (assuming uniform temperature inside the bed, as experimentally verified for several fluidized-bed reaction systems). The material balance is performed for each element *dz*, for each chemical component and for each phase, and is structured as reported in Equation (1).

$$\frac{\partial F_i(z)}{\partial z} = A \cdot \rho_{cat} \cdot \sum_{j}^{NR} r_j(z) \cdot \nu_{j,i} \pm A \cdot \delta_b(z) \cdot K_{be}(z) \cdot \left(C_{i,b}(z) - C_{i,e}(z)\right) - F_{H_2,perm}(z)$$

Equation 1

Each balance considers the variation in the molar flow of each component F_i from the inlet to the outlet of each element, depending on different terms: the first term considers the component production/consumption in chemical reactions, calculated for each reaction *j* of the total number of reactions taken into account, *NR*. In this work, the reactions included in the model are *methane steam reforming* (R.1), *water gas shift* (R.2) and *methane oxidation* (R.3).

$$CH_4 + H_2O \leftrightarrow CO + 3H_2 \quad \text{R.1}$$

$$CO + H_2O \leftrightarrow CO_2 + H_2 \quad \text{R.2}$$

$$CH_4 + 2O_2 \rightarrow CO_2 + 2H_2O \quad \text{R.3}$$

The chemical reaction term depends on the mass of catalyst at each axial position z, given from the product of catalyst apparent density ρ_{cat} (that is, particle density multiplied by reactor void fraction) and the reactive area A, the reaction rate of each reaction ($r_{j,i}$) and the stoichiometric coefficient of the component i in the reaction j ($\nu_{j,i}$), considered positive for products, negative for reactants and zero for components not involved in that reaction. For reactions R.1 and R.2, reaction rates are taken from Ref. [30], while their parameters are taken from Ref. [15] and reported here in Equation (2) and Equation (3) respectively. Reaction rates are calculated from partial pressure of reactants and products p_i and from an Arrhenius-type coefficient including a pre-exponential factor (k_j^0) and an exponent which considers the activation energy ($E_{act,j}$) over the product between universal gas constant (*R*) and reactor

temperature (T). For R.3, since methane oxidation is in general much faster than the other two reactions and it resulted from kinetic modelling that all oxygen in consumed within the first 5 cm (where membrane region start), it is assumed that all oxygen fed to the reactor instantly oxidises methane at the reactor inlet, to reduce computational efforts and improve convergence.

$$r_{R.1}(z) = \frac{k^0_{SMR} \cdot exp\left(\frac{-E_{a,SMR}}{R \cdot T}\right) \cdot \left(p_{CH_4}(z) \cdot p_{H_2O}(z) - \frac{p^3_{H_2}(z) \cdot p_{CO}(z)}{K_{eq,SMR}}\right)}{p^{1.596}_{H_2O}(z)}$$

Equation 2

$$r_{R.2}(z) = \frac{k^0_{WGS} \cdot exp\left(\frac{-E_{a,WGS}}{R \cdot T}\right) \cdot \left(p_{CO}(z) \cdot p_{H_2O}(z) - \frac{p_{H_2}(z) \cdot p_{CO_2}(z)}{K_{eq,WGS}}\right)}{p_{H_2O}(z)}$$

Equation 3

The kinetic term is zero if the balance is applied to the bubble phase or if an inert component, such as nitrogen, is considered. The total amount of solids is computed directly by the model, once specified particle density and diameter, by means of a correlation which relates the void fraction in minimum fluidization condition and the fluid dynamics, reported in Ref. [21]. A fraction of the total amount of solids is constituted of catalyst particles (Nickel or Rhodium formulation over an alumina support), while the remaining part is constituted of inert alumina support particles. Both types of particles are assumed to have the same density and diameter, as experimentally verified. Values used in this work are for a Ni-based catalyst, but, considering that catalyst amount assumed is enough to reach maximum conversion, similar results can be obtained with a lower amount of Rh-based catalyst. The ratio between catalytic particle and filler particle is set to 50% for Ni-based catalyst, while 1/10 is sufficient for Rh-based catalyst, considering its high activity.

The second term in Equation (1) is the flux between the bubble and the emulsion phase, driven by concentration difference in bubble ($C_{i,b}$) and emulsion ($C_{i,e}$). In this relation, the plus holds when the balance is performed on the emulsion phase, while the sign is minus if applied to the bubble phase. δ_b is the bubble fraction in the bed and K_{be} the exchange coefficient: both terms depend on fluidization conditions and are estimated using correlations reported in Ref. [21]. The last term of Equation (1) is hydrogen permeated for unit length ($F_{H_2,perm}$) at each axial position z and should be included only when the mass balance is applied to component hydrogen. The amount of hydrogen permeated for unit membrane area in each element ($J_{H_2,perm}$) is calculated using the Richardson's equation, reported in Equation (4), where the driving force is the difference in hydrogen partial pressure between retentate side of the membrane ($p_{H_2,retentate}$) and permeate side of the membrane ($p_{H_2,permeate}$). Flux depends on an exponent n and an Arrhenius-type permeance, characterized by a pre-exponential permeance coefficient ($Per^0_{H_2}$) and an activation energy ($E_{a,perm}$), that can be derived from permeation experiments.

$$J_{H_2,perm}(z) = Per^0_{H_2} \cdot exp\left(\frac{-E_{a,perm}}{RT}\right) \cdot \left(p^n_{H_2,retentate}(z) - p^n_{H_2,permeate}(z)\right)$$

Equation 4

Table 2 – Reactor, membranes and catalyst parameters.

Parameter	Value	Units
Reactor length	50	cm
Membrane length	45	cm
Membrane diameter	1.4	cm
Distance between membrane centers	3.4	cm
Density solid particle	2000	kg/m^3
Diameter solid particle	180	μm
k^0_{SMR}	$9.43 \cdot 10^5$	kmol/(h·kg·bar$^{0.404}$)
$E_{a,SMR}$	106.9	kJ/mol
k^0_{WGS}	$8.82 \cdot 10^2$	kmol/(h·kg·bar)
$E_{a,WGS}$	54.5	kJ/mol
$Per^0_{H_2}$	9.94	kmol/(h·m·bar$^{0.5}$)
$E_{a,perm}$	9.26	kJ/mol
n	0.5	–

This term is related to the last term of Equation (1) from the following relation (Equation (5)), which express the hydrogen permeated for unit of membranes length, considering the number ($N_{membranes}$) and diameter of the membranes ($d_{membrane}$).

$$F_{H_2,perm}(z) = N_{membranes} \cdot \pi \cdot d_{membrane} \cdot J_{H_2,perm}(z)$$

Equation 5

Geometric parameters of the reactor and of the membranes, as well as kinetic parameters for reaction rates equations and membrane parameters for permeation behaviour, are reported in Table 2.

Compared to the previous works, here the algorithm and the fluidization model have been improved. Mainly, the ordinary differential equations convergence have been re-written using ACM tools to optimize the solutions and the accuracy of the solution was refined increasing the reactor discretization and the order of convergence of the differential equations implemented in the model, assuring a good compromise between convergence time and grid independent results. The decisions of the number of grid points came from preliminary analysis, performed with different order of convergence and convergence method. Firstly, the amount of hydrogen permeated through the membrane is calculated at different grid points, using the highest level of accuracy, provided in ACM by a UPwind-based Backward-Difference method of the 4th order (UPBD4). Results are reported on the left of Fig. 3, and shows that the results on the amount of hydrogen permeated are grid independent above 500 points. For a lower number of points, production is slightly underestimated (about 1% less working with 100 points).

To reduce the computational effort, an additional analysis investigated the results with different convergence methods. The comparison was between three finite-difference methods with different order of convergence (BDF1, BDF2, UPBD4, all based on backward difference) and a finite-elements method (OCFE2). Last number in the name indicates the order of convergence. Results, reported on right side of Fig. 3, showed that above 250 points all methods guaranteed a reasonable accuracy (below 0.5%), with the error halved going from 1st to 2nd order method and substantially unchanged for higher orders. Thus, it has been decided to use 250 grid points and a 2nd order method (BDF2).

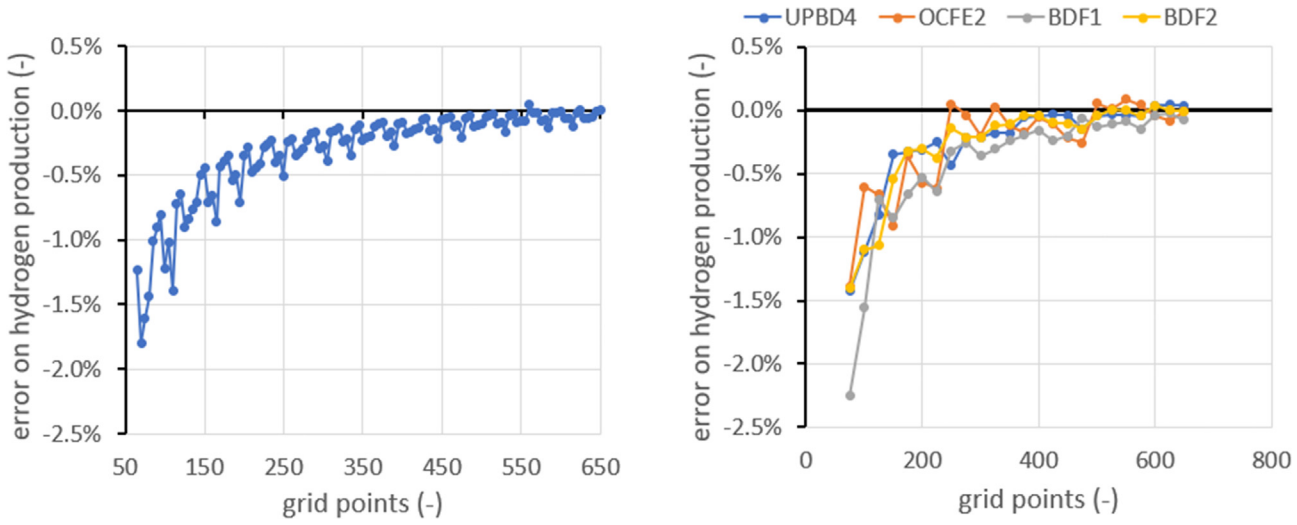

Fig. 3 – Preliminary analysis on equations convergence to select the number of grid points and the method and order of convergence. Results on the left are obtained with UPBD4 method, which guarantees maximum accuracy. (For interpretation of the references to color in this figure legend, the reader is referred to the Web version of this article.)

Regarding the bubble-emulsion phase behaviour, the description of the bubble wake was added (wake phase). As in the previous version, the model neglects concentration polarization losses, because no correlations are available for fluidized bed with vertical membranes and, according to experimental test on lab test prototype, it can be expected their influence is lower at large scale compared to smaller reactors. Possible mass transfer limitations in the membrane support are also neglected.

System layout and assumptions

The system layout for both the investigated feedstocks is reported in Fig. 4. Compressed BG/BM is mixed with compressed air and then preheated up to maximum 300 °C to avoid methane cracking. Just before reactor inlet, biogas-air mixture is mixed with steam and enters the reactor. The steam is produced from water at ambient conditions, pumped until reactor pressure and heated in three heat exchangers (HX-1, HX-2, HX-3), reaching a temperature above 500 °C, to end up with a feed temperature of about 400 °C at the reactor inlet and thus avoiding strong thermal gradients within the reactor. Inside the reactor, the oxidation reaction will rise the temperature up to 550 °C and, in addition, will provide the heat required by the reforming reactions. In the fluidized-bed reactor, no temperature gradient is considered and an isothermal profile along z is assumed. Permeate flow, consisting of pure hydrogen, and retentate flow are then both at 550 °C. Permeate is cooled down in two heat exchangers: the first one provides heat for to steam superheating (HX-3), and the second one to the water preheating (HX-1). Once cooled down, the permeated hydrogen is led to atmospheric pressure by two-stages refrigerated vacuum pump and then compressed with an intercooled compressor up to 20 bar. This choice of the delivery pressure has been done to be consistent with previous works and has no effect in the BG/BM cases comparison since pure hydrogen production is fixed, and then the amount of energy required for H_2 compression is the same

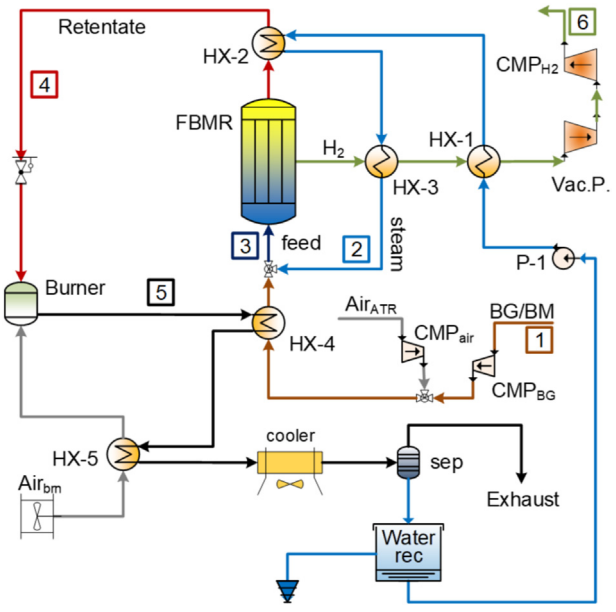

Fig. 4 – System layout.

in both cases. The retentate flow is cooled down in HX-2 to provide the heat for steam production, then it is throttled to atmospheric pressure and sent to a catalytic burner to complete the oxidation of CO, H2 and CH4. These reactions provide additional heat to the flue gases, used for the BG/BM preheating (up to 300 °C) and for the air pre-heating.

Manipulated variables are the feed pressure, the reactor diameter and the number of membranes inserted in the reactor. Feed pressure investigated are 10, 12 and 14 bar, consistently with the results obtained in a previous work for the same system [23]; reactor diameters investigated go from 36 cm to 45 cm, since it is a range that ensure correct fluidization and correct fitting of all the membranes. The number of membranes reported is from 70 to 134, since for lower values the drop in efficiency is in all cases very relevant and

Table 3 – Example of main streams of BG case with 120 membranes.

Stream	Flow		T (°C)	p (bar)	Composition (% molar basis)						
	Molar (mol/s)	Mass (g/s)			CH_4	H_2	CO	CO_2	H_2O	O_2	N_2
1	0.333	8.717	50	1	58.1	0	0	33.9	3.1	1.1	3.8
2	0.292	5.266	520.5	10	0	0	0	0	100	0	0
3	1.032	25.725	363.3	10	18.7	0	0	10.9	29.3	8.6	32.4
4	0.753	24.568	198.8	10	0.1	1.2	1.1	39.4	13.8	0	44.4
5	1.001	32.156	333.5	1	0	0	0	30.4	11.4	4.5	53.8
6	0.574	1.157	141.3	20	0	100	0	0	0	0	0

Table 4 – Example of main streams of BM case with 70 membranes.

Stream	Flow		T (°C)	p (bar)	Composition (% molar basis)						
	Molar (mol/s)	Mass (g/s)			CH_4	H_2	CO	CO_2	H_2O	O_2	N_2
1	0.203	3.424	50	1	96.0	0	0	2.0	0	0.5	1.5
2	0.319	5.751	324.7	14	0	0	0	0	100	0	0
3	0.943	21.305	339.3	14	20.7	0	0	0.4	33.9	9.5	35.6
4	0.664	20.148	163.6	14	0.4	1.7	0.9	28.7	17.9	0	50.5
5	0.902	27.249	378.8	1	0	0	0	22.1	15.0	4.2	58.7
6	0.574	1.157	141.3	20	0	100	0	0	0	0	0

for higher values the costs rise without additional benefits. An example of typical flow rates and compositions of the main streams are reported in Table 3 for BG and in Table 4 for BM. Cases selected are two limit cases: for BG, main streams are reported at 10 bar and with 120 membranes. For BM, at 14 bar and with 70 membranes.

The assumptions for the system are mainly taken from Ref. [23] and are reported in Table 5. The maximum number of membranes for each case is tied to reactor diameter, since the minimum distance between membranes centers is fixed to 3.4 cm, and thus for smaller diameters only a limited number of membranes fit into the reactor. The center-center distance selected derives from the consideration that at least 2 cm of space should be left between the membranes to avoid a strong increase of the concentration polarization losses [31], and adding the membrane outer diameter, which is 1.4 cm. To ensure a correct fluidization of the bed, it should be verified that the gas velocity stays in a certain range: in this work, the range allowed of the ratio between superficial velocity u and minimum fluidization velocity u_{mf} is between 1.5 and 5. The lower boundary is to be conservative in avoiding defluidization. The fastest boundary is chosen to be conservative on avoiding the removal of catalyst particles from the reaction zone due to an increase in the gas drag force.

Table 5 – System assumptions for the simulations.

Fixed parameter	Value	Units
Reactor uniform temperature	550	°C
Vacuum side pressure	0.1	bar
Steam-carbon-ratio at $x = 5\,cm$	3	–
Fluidization (u/u_{mf}) range	1.5 → 5	–
Hydrogen production	100	kg/day
Hydrogen delivery pressure	20	bar
Ambient temperature	25	°C
Controller consumption (% of total auxiliary consumption)	10	%
Average electric efficiency of the power generating park	45	%
Water pump hydraulic/mechanical efficiency	0.7/0.9	–
Vacuum pump isentropic/mechanical efficiency	0.7/0.85	–
Compressors isentropic/mechanical efficiency	0.7/0.85	–
Minimum ΔT in heat exchangers	30	°C
Heat transfer coefficient gas/gas	60	$W/(m^2 \cdot K)$
Heat transfer coefficient gas/liquid-biphasic	70	$W/(m^2 \cdot K)$
LHV_{H2}	120	MJ/kg
Investigated parameter	**Value**	**Units**
Retentate pressure	10 -12 - 14	bar
Reactor diameter	36 → 45	cm
Number of membranes	70 → 134	–

Regarding the reactor feed inlet, BG/BM flow rate is set in order to produce the target amount of pure hydrogen, while the steam flow rate is set such that the *steam-carbon-ratio*, defined as the ratio between steam and methane molar flows in the feed, is fixed at the beginning of the membrane region, to avoid carbon deposition over the catalyst and over the membrane surface. Experimental results [15] show that a value of 3 should be enough conservative. Air flow rate to the reactor is tuned to obtain autothermal conditions within the reactor. On the other hand, the air flow rate to the catalytic burner is instead set in excess to have an oxygen molar fraction in the dry flue gases equal to 5%.

Key performance indicators

To evaluate the performance and to compare the different feedstocks, mainly two indicators are used. From the reactor point of view, the efficiency parameter investigated is the *Hydrogen Recovery Factor* (HRF), defined as the ratio of moles of hydrogen separated (n_{H_2}) through the membrane (so the pure hydrogen produced) with respect to the total ideal

hydrogen production obtained under the hypotheses that: i) all methane fed to the reactor and available for reforming is converted to H_2 and ii) all hydrogen produced in the reforming reactions is separated through the membranes. HRF is defined in Equation (6). The expression for the denominator becomes clear considering that, through reactions R.1 and R.2, for each mole of methane that undergoes to reforming ($n_{CH_4,in}$), 4 mol of hydrogen can be obtained; in the meantime, 1 mol of methane is burned every 2 mol of oxygen fed to the reactor and then the moles of methane that do not go to reforming are half the moles of oxygen fed ($n_{O_2,in}$).

$$HRF = \frac{n_{H_2}}{4 \cdot \left(n_{CH_4,in} - \frac{n_{O_2,in}}{2}\right)} \quad \text{Equation 6}$$

At system level, the HRF alone is no longer the best indicator to identify the best design point and it could instead be useful to refer to an energy efficiency of the system, defined as the energy output associated to the hydrogen produced over the total power inlet to the process. The energy input to this process is due to the biogas/biomethane fed and to the primary energy necessary to produce the electric energy for auxiliaries' consumptions. The system efficiency (η_{system}) and the Specific Energy Consumption (SEC) are defined in Equation (7) and Equation (8) respectively. LHV for hydrogen, biogas and biomethane are respectively 120 MJ/kg, 17.8 MJ/kg and 45.7 MJ/kg. The terms m_{H_2} and m_F refer to the mass flow of hydrogen permeated and mass flow of feedstock sent to the reactor respectively.

$$\eta_{system} = \frac{m_{H_2} \cdot LHV_{H_2}}{m_F \cdot LHV_F + \frac{W_{aux}}{\eta_{el,ref}}} \quad \text{Equation 7}$$

$$SEC = \frac{LHV_{H_2}}{\eta_{system}} = \frac{m_F \cdot LHV_F + \frac{W_{aux}}{\eta_{el,ref}}}{m_{H_2}} \quad \text{Equation 8}$$

System performance

The effect of manipulated variables (retentate side pressure, reactor diameter and number of membranes) on reactor and system performance was investigated in a series of analyses both for the BG and BM cases. The trends are firstly reported for BG case. Comparison between BG case and BM case is reported in section 3.2.

System efficiency and HRF trends

Results of the analysis of the reactor behaviour are reported in terms of HRF at the left of Fig. 5. Clearly, by increasing the number of membranes, the HRF increases as well, since there is more membrane area available for hydrogen to permeate. The positive effect of an additional membrane is always lower as the number of membranes increases, until HRF reaches an asymptote. The increase of the reactor diameter leads also to an increase of the reactor efficiency, and this is mainly due to the reduction in the gas velocity due to the increased cross section area. Reduction in gas velocity leads to a higher residence time and therefore to higher conversions. This effect is of course limited to the fact that the fluidization regime should be guaranteed. In the investigated range, also the effect of pressure increase is beneficial for the reactor. In general, reforming reactions are penalised by high pressure since they occur with an increase of total number of moles of the system. Nevertheless, higher pressures entail lower velocities – due to reduction of gas density and then volumetric flow - and then an increase in the residence time. Most important, in membrane reactors, an increase in pressure has the beneficial effect of increasing the hydrogen partial pressure at the retentate side, and then the driving force for hydrogen permeation. In this case, driving force gain effect overcomes the drop in equilibrium conversion. Ideally, with an infinite number of

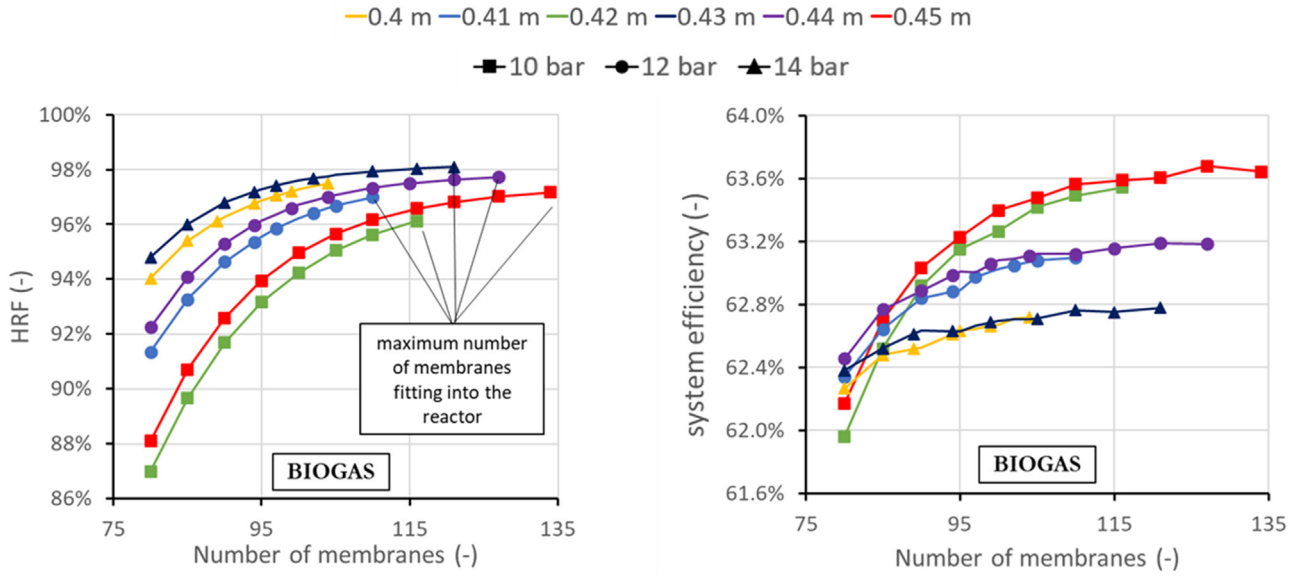

Fig. 5 – Effect of feed pressure and reactor diameter on hydrogen recovery factor (left) and system efficiency (right) for different number of membranes inserted in the membrane reactor.

membranes fitted into the reactor, all the curves reaches the same asymptotic value of HRF, obtained when hydrogen has the same partial pressure at both sides of the membranes.

The reactor results anyhow do not take into account heat integration and auxiliaries' consumption of the overall plant. Thus, they cannot by themselves identify the best working point of the system. For this reason, also the system efficiency is evaluated. Results are reported on the right of Fig. 5. From the system point of view, reactor diameter influence is negligible. The trend of pressure is reversed: in general, lower operating pressures lead to higher system efficiencies compared to higher pressures. This trend cannot be considered as a general rule and it is influenced by the reactor design: in this case, below 110 membranes the efficiency slope at 10 bar become steep, while at 12 bar it happens with 85 membranes. For this reason, at about 90 membranes the curves cross each other and then below this value the higher-pressure case has an higher efficiency. The same discussion could be done for other pressure values. More interesting is the other side of the chart: by increasing the number of membranes, the curves reach an asymptotic value of efficiency, due to the steadiness of HRF. The difference, in this case, is that such asymptotic values depend on the operating pressure and are higher for lower pressure: for 14 bar, maximum value is 62.6%; for 12 bar, 63.2% and for 10 bar 63.6%. This behaviour can be explained considering that by increasing the number of membranes, the HRF becomes the same for all pressures. Since hydrogen production is fixed, the equivalence of HRF means the same amount of biogas fed to the reactor. Then, the only different term in Equation (7) among the cases is the power required by the auxiliaries at the denominator. The difference is mainly due to the increased power required by air and biogas compressors at higher pressures.

Simulations results of right-side of Fig. 5 appear wobblier compared to left-side figure since they refer to the overall system. In simulations at system level, different design specs are defined in AP to match the desired constraints (set values of hydrogen production, reactor thermal duty and steam-carbon-ratio), as well as the minimum temperature differences in the heat exchangers. Design specs have a certain tolerance, which leads to a small floating of the results, which does not appear in the curves at reactor level (left side). However, the trends obtained at system level are in all cases clear.

Since the trends in terms of HRF and system efficiency lead to different conclusions, it can be interesting to compare the two curves of one case study, so fixing reactor diameter and operative pressure. As already stated, for a large number of membranes both curves reach a plateau. It is however clear from Fig. 6 that system efficiency reaches the plateau for a lower number of membranes. This effect holds for a relevant number of membranes: in this example, HRF has not already reached the plateau with 127 membranes while system efficiency is about constant already at 95 membranes. The reason for that can be found in the fact that when HRF decreases, retentate flow is richer of unconverted methane and hydrogen, and thus it is characterized by a higher LHV. Then, when the retentate is oxidized in the catalytic burner, there is an additional heat recovery which, in end, increases the temperature of the feed that enters the reactor. In case of Fig. 6, for example, with 127 membranes the retentate combustion can provide heat to bring the reactor feed at 335 °C, while with 85 membranes it can reach 414 °C. This allows to save a certain amount of air fed to the reactor and then to decrease the air compressor power duty (4.9 kW with 127 membranes vs 4.6 kW with 85 membranes).

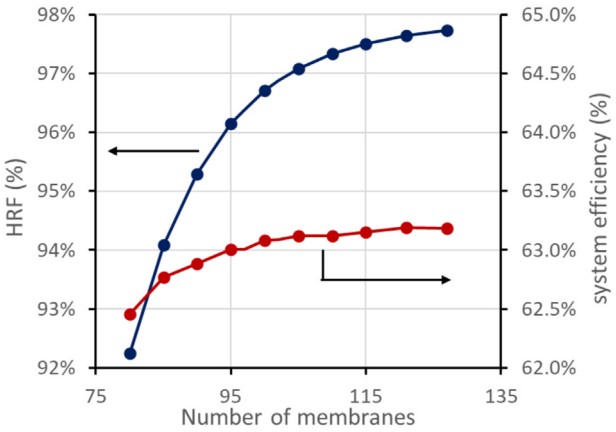

Fig. 6 – Typical trends of HRF (blue) and system efficiency (red) for different number of membranes. Results obtained at 12 bar and 44 cm of reactor diameter. (For interpretation of the references to color in this figure legend, the reader is referred to the Web version of this article.)

Comparison between biogas and biomethane

Same charts presented above can be obtained using biomethane as feedstock of the system. In this case, the absence of inert carbon dioxide in the reactor feed increases the hydrogen molar fraction then the driving force for permeation, depending on its partial pressure. In general, the effect of manipulated variables are the same already reported for biogas. It is then only relevant a comparison with biogas results. The results, shown in Fig. 7, clearly show that biomethane outperforms biogas both from the point of view of the reactor and the overall system. In terms of HRF, at fixed reactor diameter and number of membranes, the two positive effects of using biomethane instead of biogas, driven by the absence of nitrogen, are the increase in hydrogen partial pressure and the reduction of fluidization velocity. The latter effect is due a reduction of the molar (and then volumetric) flow required, since the analysis is performed at fixed hydrogen production. The advantages in using biomethane are reduced by increasing the number of membranes: with 121 membranes and 43 cm reactor, for example, HRF is 98.7% for BM and 98.1% for BG. With same diameter and 85 membranes, HRF for BM is 98.1% while for BM 96.0%. A similar trend was observed for the other pressures investigated, with the same effect already reported for biogas case.

As discussed in the previous section, an increase in HRF is not obviously related to an increase in system efficiency. In this case however, biomethane outperforms biogas also from the point of view of the overall system. Asymptotic value at 14 bar, for example, is 63.8% for BM and 62.8% for BG, as shown at the right side of Fig. 7. The reason for its higher value is mainly the electric energy saving in the power required for BM compression. In the asymptotic region at 14 bar, BG compressor requires 4.4 kW while BM compressor only 2.7 kW.

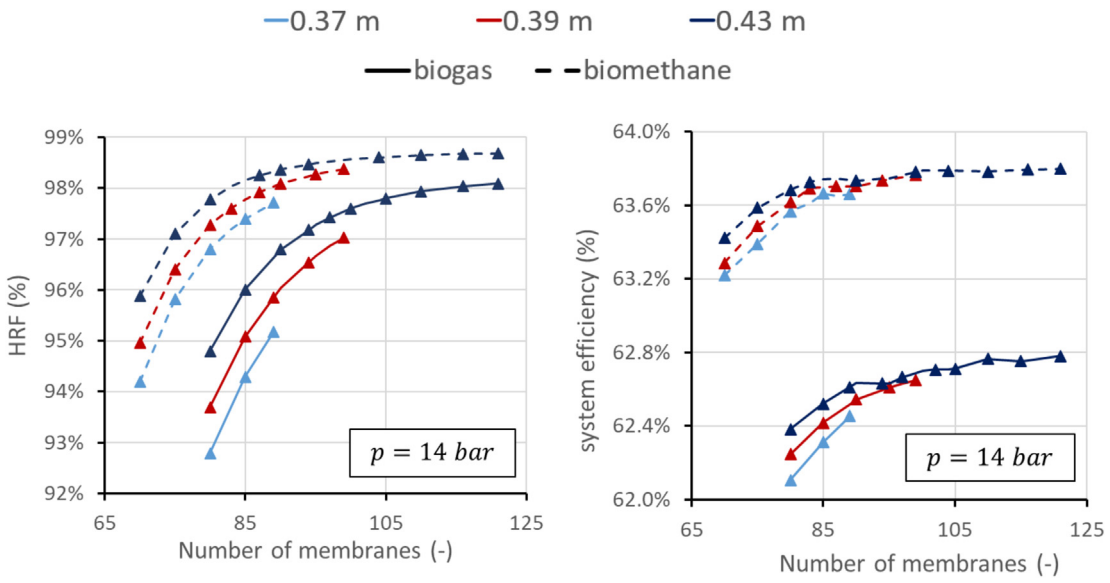

Fig. 7 – Comparison between biogas and biomethane in terms of HRF (left) and system efficiency (right) for different reactor diameters and number of membranes at 14 bar.

From a pure technical point of view, a design criterion for the reactor can be to work at the beginning of the plateau of system efficiency, where the increase in membrane numbers can potentially reduce the reactor reliability, increase the investment and maintenance costs without any additional benefit on the overall system. So the biomethane case would lead to 85 membranes with an efficiency of about 63.7%, while biogas case required 95 membranes with an efficiency of 62.6%. Nevertheless, a better criterion will be given from the economic analysis in section 4, to evaluate if it is worth to trade some efficiency to work with lower membranes, then having a feedstock extra cost but a reduction in membranes cost.

Economic analysis

An economic analysis is carried out to estimate the hydrogen production cost using both the feedstocks. The approach and the main assumptions are mainly taken from Ref. [22], and it consists in the evaluation of the *Levelized Cost Of Hydrogen* (LCOH). Assumptions for standard components are consistent with [22], while assumptions for the membrane reactor are consistent with [23].

Methodology and assumptions

For the economic analysis, the parameter identified to optimize the process is the LCOH, evaluated in €/kg, defined as in Equation (9). The evaluation of the cost of hydrogen production is composed by the total plant cost (TPC) and the Operations and Maintenance (O&M), fixed and variables, divided by the mass flow rate of hydrogen produced. The TPC is converted in an annual operating cost using the Capital Charge Factor (CCF) methodology. 7500 working hours (h_{eq}) are considered.

$$LCOH = \frac{TPC \cdot CCF + O\&M_{fix} + O\&M_{var} \cdot h_{eq}}{m_{H_2}} \quad \text{Equation 9}$$

The TPC is calculated starting from basic components cost (C_i) and then adding installation costs (TIC), indirect costs (IC) and owner's and contingencies costs (C&OC), according to Equation (10). Basic component costs were available for some reference sizes and were scaled up using CEPCI index method, as in Equation (11), based on their actual size (S_i), starting from a reference cost ($C_{i,0}$) at the reference size ($S_{i,0}$).

$$TPC = \left(\sum_i C_i\right) \cdot (1 + \%_{TIC}) \cdot (1 + \%_{IC}) \cdot (1 + \%_{C\&OC}) \quad \text{Equation 10}$$

$$C_i = \left(C_{i,0} \cdot \left(\frac{S_i}{S_{i,0}}\right)^f\right)_y \cdot \frac{CEPCI_{2020}}{CEPCI_y} \quad \text{Equation 11}$$

The economic purpose is clearly to identify the operating conditions and reactor geometries which minimize the LCOH.

In this work, heat exchangers cost has been refined, such as the calculation of heat exchangers area, based on the UA value provided by AP and then assuming typical values for heat transfer coefficient U to determine heat exchanger area, reported in Table 5. BM cost have been taken from Ref. [8] as the world average value, and is 19 $/MBtu, corresponding to 0.532 €/Nm^3. BG cost is then estimated considering an average upgrading cost of 3 $/MBtu [32] and subtracting it to BM cost. It results 16 $/MBtu, corresponding to 0.2712 €/Nm^3, and it is consistent with [8]. Due to the simplicity of the system, labor cost estimated is 30 k€/y.

CEPCI index have been updated to the 2020 value, which is 596.2 [33]. Main economic assumptions, together with the parameters for the calculation of TPC of Equation (10), are reported in Table 6.

Table 6 – Main economic assumptions on O&M, TPC and feedstock costs.

Parameter	cost	unit
Biogas cost	16–0.2712	$/MBtu - €/Nm^3
Upgrading cost	3	$/MBtu
Biomethane cost	19–0.532	$/MBtu - €/Nm^3
Catalyst	540	k€/m^3
Filler	50	k€/m^3
Electric energy	0.12	€/kWh
Maintenance	2	% of TPC
Insurance	2.5	% of TPC
Annual labour cost	30	k€
CCF	0.16	–
%TIC	0.65	–
%IC	0.14	–
%C&OC	0.15	–
$CEPCI_{2020}$	596.2	–

LCOH trend

Trends of LCOH for different pressures, reactor diameters and number of membranes are reported on the left side of Fig. 8. At the same reactor diameter, the minimum in LCOH values is similar at all pressures, but in general higher pressures allows to reach the minimum at a lower number of membranes, which is preferred since membranes are a breakable component in the reactor. At higher pressure, HRF is higher so less biogas is required at fixed hydrogen production. On the other side, higher pressures have lower system efficiency, that means a higher cost for electricity. The preference in working at higher pressures allows also to adopt smaller diameters (gas density reduces) and an increase of the LCOH is associated with the increased reactor diameter since additional material will be necessary for its realization and more catalyst fits into the reactor. However, this advantage is limited since reducing reactor diameter also means that less membranes can be fitted into the reactor.

The LCOH curve shows a parabolic trend if plotted as a function of the number of membranes. With a low number of membranes, the rise in the LCOH is mainly due to the additional feedstock cost. In this region, the HRF is low, and then a higher amount of BG/BM is needed to reach the target of 100 kg/day. Moreover, more heat is available in the retentate and then a higher heat exchanger area results from the calculation, with an increase in plant cost. By increasing the number of membranes, the effect of the increase of HRF for an additional membrane is always smaller. The LCOH decreases since feedstock cost is reduced, while increases due to the additional cost of membranes. After the minimum, cost of the membranes progressively overtake the savings in feedstock cost.

Comparison between biogas and biomethane

Comparison in terms of LCOH between BG and BM is shown on the right side of Fig. 8. For both feeds, the shape of the curve is the same previously discussed: it has a parabolic behaviour as a function of number of membranes, and LCOH is higher for higher reactor diameters. It turns out clearly that BM leads in any case to a higher LCOH. The minimum is obtained, in BM case, for a lower number of membranes and a smaller reactor diameter.

Results for the best design case of both feeds are reported in Table 7, together with the power balances and the flow rates of some relevant streams of the system. The composition of LCOH for the best design identified in BG and BM case is reported in Fig. 9. As expected, using BM as feedstock, the TPC is reduced due to lower membrane reactor cost and lower cost for gas compressor. There is also a reduction in electricity cost, due to the lower electric consumption of the gas

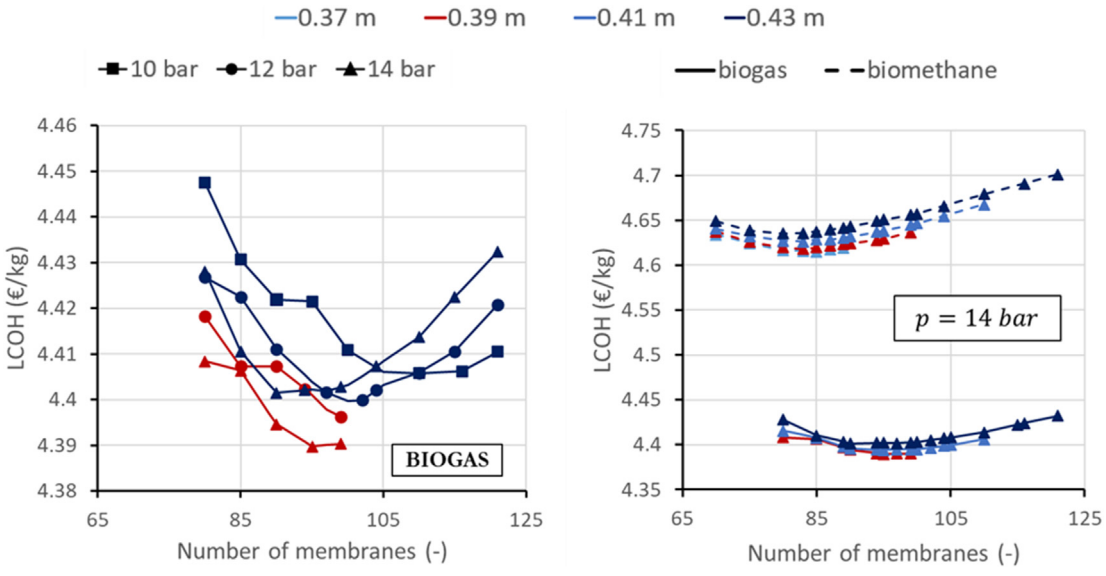

Fig. 8 – On the left, typical trend of LCOH, reported for biogas case, as a function of the number of membranes for different pressures and reactor diameters. On the right, comparison, at 14 bar, of LCOH curves for biogas and biomethane.

Table 7 – Comparison of results in the best-design case for the different feedstocks.

Parameter	Biogas	Biomethane
Reactor temperature (°C)	550	550
Retentate pressure (bar)	14	14
Vacuum side pressure	0.1	0.1
Reactor diameter (cm)	39	37
Number of membranes (–)	99	85
Gas feed (Nm^3/h)	26.8	16.2
Water flow rate (kmol/h)	1.07	1.11
Air (to reactor) flow rate (kmol/h)	1.48	1.56
Air (to burner) flow rate (kmol/h)	0.90	0.78
BG/BM compressor power (kW)	4.42	2.69
Air compressor power (kW)	5.21	5.47
Vacuum pump power (kW)	8.57	8.57
Water pump power (kW)	0.01	0.01
H_2 compressor power (kW)	8.36	8.36
Thermal power for steam production (kW)	24.38	21.51
Thermal power exchanged HX-4 (kW)	3.21	2.14
Thermal power exchanged HX-5 (kW)	1.23	1.05
Total electric requirement (kW)	29.23	27.60
Gas power input (kW)	155.0	155.1
H2 power output (kW)	137.8	137.8
Hydrogen production (kg/day)	100	100
HRF (%)	97.0	97.4
System efficiency (%)	62.7	63.7
SEC (kWh/kg)	53.2	52.4
LCOH (€/kg)	4.39	4.62
LCOH (€/MWh)	132.7	139.5

compressor, which is about halved. Nevertheless, the additional cost of the feedstock is greater than these reduction effect, making in the end BG the preferred choice.

Sensitivity analyses

The limited TRL of the membrane reactor technology entails many uncertainties on the membrane reactor cost; for this reason, a set of sensitivity analyses has been performed to investigate the impact of membranes, reactor and catalyst costs on the LCOH. Reactor cost (without membranes nor catalyst) is now set to 3.5 times the raw material cost, but it is here investigated from 2 to 15 times of material cost. Membrane cost is investigated if halved or doubled. Catalyst costs is halved or multiplied by a factor 4. Other parameters investigated are the annual labour cost to 60 k€ (currently 30 k€), also difficult to be evaluated in this stage, and the feedstock cost. The latter parameter has been varied in the range of the BG production cost available [8], since it has been chosen for this work an average cost, but it can be very different depending on the situation. For BG it goes from 0.136 €/Nm^3 to 0.364 €/Nm^3 (currently 0.2712 €/Nm^3) and for BM from 0.266 €/Nm^3 to 0.72 €/Nm^3 (currently 0.532 €/Nm^3). The BM cost is directly related to BG range, obtained by adding to the BG cost a fixed upgrading cost.

Dealing with vacuum hydrogen requires high-grade steels components for which still hold uncertainties in their costs. A

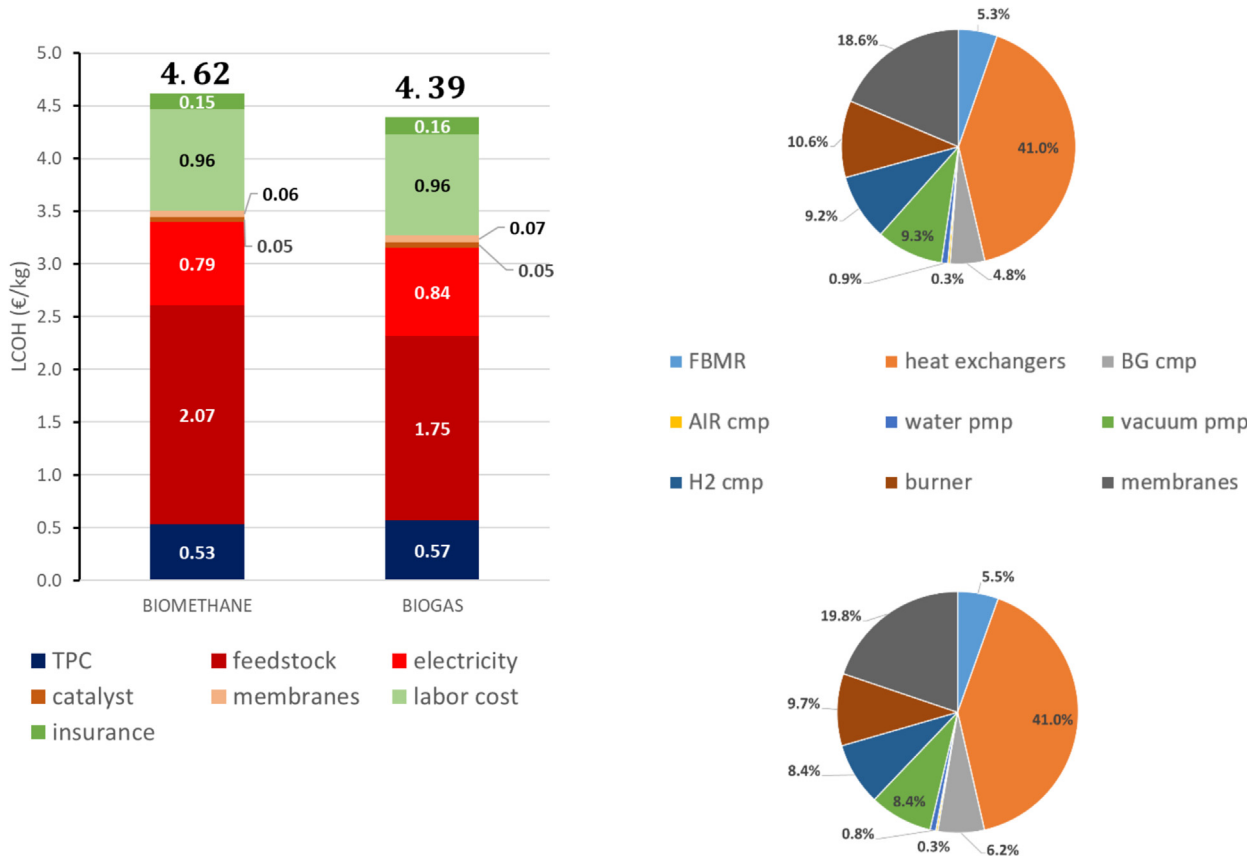

Fig. 9 – On the left, LCOH comparison for BG vs BM divided in its components; on the right, TPC composition for BM (top) and BG (bottom).

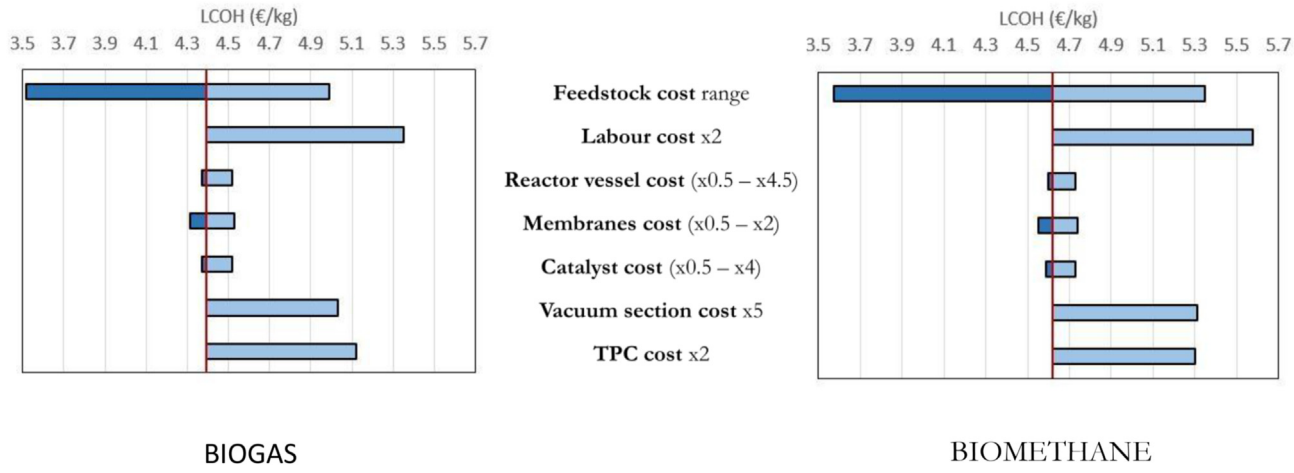

Fig. 10 – Sensitivity analysis on LCOH for some relevant parameters.

sensitivity analysis has been then performed to investigate the influence of components cost on vacuum section (vacuum pump, heat exchangers ECO and SH and the hydrogen compressor) on final LCOH calculated in the two solutions. The cost is investigated up to 5 times the value calculated by correlations, and the relative advantage of biogas over biomethane is confirmed, with a LCOH increase up to 5.03 €/kg_{H2} and 5.31 €/kg_{H2} respectively. Similarly, an analysis on TPC influence over total cost has been performed by due to further possible under-estimations. Doubling TPC will end up in a final LCOH of 5.12 €/kg for biogas and 5.30 €/kg for biomethane. Again, the relative advantage of biogas over biomethane holds. In this case, the share of TPC on final LCOH goes from 13% to 22%.

The sensitivity analysis, which results are presented in Fig. 10, shows again the important impact of the feedstock cost in the final LCOH. Effect of costs of the MR components is instead limited. Regarding the shape of LCOH charts and the new optimum design point, changes in feedstock cost or in labour cost or in catalyst cost has no influence, so the optimum point is always at 14 bar and for the diameter and number of membranes listed in Table 7, depending on BG or BM cases. Also in the case of an increase of the reactor cost, the optimum remain the same in terms of pressure and number of membranes. Regarding the diameter, it is relevant to state that in this case the influence is higher than in the reference case considered: with 15 times the raw material cost, generally an increase of 1 cm in reactor diameter leads to an increase of 0.01 €/kg in LCOH. For the membranes, a variation in the cost has also an influence on the shape of LCOH curves: considering a double cost, the minimum moves towards lower number of membranes (90 for BG, 75 for BM); if the cost is halved, minimum LCOH is obtained at 105 membranes in BG case while it stays constant at 85 membranes in BM case. Optimum pressure is, in all cases, 14 bar.

Maintaining the same parameters used in this analysis, it is also possible to estimate what should be the average cost of upgrading to reach the same LCOH. It turned out that it should be 2.84 €/MWh (0.97 $/MBtu), so a reduction of about 70% compared to the current average cost, which is 8.79 €/MWh (3 $/MBtu).

Conclusions

This work presented a tecno-economic assessment of a small-scale hydrogen production plant using membrane reactor technology. The analyses have been performed for different pressures, reactor diameters and number of membranes with the aim of investigating the trends in the efficiency parameters, both from the point of view of the reactor (HRF) and of the overall system (η_{system}). Moreover, a comparison between biogas and biomethane as feedstocks has been performed. Through an economic evaluation has been identified the best design of both cases, as the one which minimize the LCOH.

From a thermodynamic point of view, it turned out that both HRF and system efficiency increase by increasing the number of membranes: the growth is sharper for lower membranes and reaches a plateau around 115–125 membranes. Higher pressures outperform lower pressure in terms of reactor efficiency but are less efficient from the point of view of the overall system. The asymptotic values are higher if biomethane is used as feedstock, due to lower inert (CO_2) presence which increases hydrogen partial pressure and thus driving force for permeation. Moreover, with lower molar flow within the reactor, the fluidization velocity decreases and this positively affects efficiency of the reactor since residence time increases.

From an economic point of view, given a certain feedstock, a higher pressure leads to minimum in LCOH at lower number of membranes. Using BM, the optimum configuration in terms of LCOH allows to work with smaller reactor and a less membranes compared to biogas, thus to reduce TPC and fixed O&M. Nevertheless, even if the amount of feedstock is reduced, with the current upgrading cost, biogas results the most convenient choice in terms of LCOH, since the higher feedstock cost exceeds savings in TPC and auxiliaries consumptions. It is anyhow important to stress that, since MRs are still being validated at TRL7, economic assumptions contain several uncertainties, that will be possibly refined along with the industrial development of the technology.

Declaration of competing interest

The authors declare that they have no known competing financial interests or personal relationships that could have appeared to influence the work reported in this paper.

Acknowledgments

MACBETH has received funding from the European Union's Horizon 2020 research and innovation program (grant agreement No 869896).

REFERENCES

[1] IEA. Net zero by 2050: a roadmap for the global energy sector. Int. Energy Agency 2021;224. Net Zero by 2050 – Analysis - IEA
[2] Electricity. World energy outlook 2019 – analysis - IEA (n.d.), https://www.iea.org/reports/world-energy-outlook-2019/electricity.
[3] International Energy Agency. The Future of Hydrogen: seizing today's opportunities. IEA Publ.; 2019. p. 203. https://www.iea.org/reports/the-future-of-hydrogen.
[4] Global hydrogen review 2021. Glob. Hydrog. Rev. 2021;2021. https://doi.org/10.1787/39351842-en.
[5] Nikolaidis P, Poullikkas A. A comparative overview of hydrogen production processes. Renew Sustain Energy Rev 2017;67:597–611. https://doi.org/10.1016/j.rser.2016.09.044.
[6] Clark D, Malerød-Fjeld H, Budd M, Yuste-Tirados I, Beeaff D, Aamodt S, Nguyen K, Ansaloni L, Peters T, Vestre PK, Pappas DK, Valls MI, Remiro-Buenamañana S, Norby T, Bjørheim TS, Serra JM, Kjølseth C. Single-step hydrogen production from NH3, CH4, and biogas in stacked proton ceramic reactors. Science 2022;376:390–3. https://doi.org/10.1126/science.abj3951.
[7] Fernandez E, Coenen K, Helmi A, Melendez J, Zuñiga J, Pacheco Tanaka DA, Van Sint Annaland M, Gallucci F. Preparation and characterization of thin-film Pd-Ag supported membranes for high-temperature applications. Int J Hydrogen Energy 2015;40:13463–78. https://doi.org/10.1016/j.ijhydene.2015.08.050.
[8] International Energy Agency, Outlook for biogas and biomethane. Prospects for organic growth. World Energy Outlook Special Report.; 2020. p. 93. https://www.iea.org/reports/outlook-for-biogas-and-biomethane-prospects-for-organic-growth.
[9] Kapoor R, Ghosh P, Kumar M, Vijay VK. Evaluation of biogas upgrading technologies and future perspectives: a review. Environmental Science and Pollution Research; 2019. https://doi.org/10.1007/s11356-019-04767-1.
[10] Scarlat N, Dallemand JF, Fahl F. Biogas: developments and perspectives in europe. Renew Energy 2018;129:457–72. https://doi.org/10.1016/j.renene.2018.03.006.
[11] Di Marcoberardino G, Binotti M, Manzolini G, Viviente JL, Arratibel A, Roses L, Gallucci F. Achievements of European projects on membrane reactor for hydrogen production. J Clean Prod 2017;161:1442–50. https://doi.org/10.1016/j.jclepro.2017.05.122.
[12] BIONICO project (n.d.), http://www.bionicoproject.eu/.
[13] MACBETH project (n.d.), https://www.macbeth-project.eu/.
[14] Brencio C, Fontein FWA, Medrano JA, Di Felice L, Arratibel A, Gallucci F. Pd-based membranes performance under hydrocarbon exposure for propane dehydrogenation processes: experimental and modeling. Int J Hydrogen Energy 2022;47:11369–84. https://doi.org/10.1016/j.ijhydene.2021.09.252.
[15] Marra L, Wolbers PF, Gallucci F, Annaland MVS. Development of a RhZrO2 catalyst for low temperature autothermal reforming of methane in membrane reactors. Catal Today 2014;236:23–33. https://doi.org/10.1016/j.cattod.2013.10.069.
[16] Wang S, Luo K, Hu C, Sun L, Fan J. Impact of operating parameters on biomass gasification in a fluidized bed reactor: an Eulerian-Lagrangian approach. Powder Technol 2018;333:304–16. https://doi.org/10.1016/j.powtec.2018.04.027.
[17] Medrano JA, Tasdemir M, Gallucci F, van Sint Annaland M. On the internal solids circulation rates in freely-bubbling gas-solid fluidized beds. Chem Eng Sci 2017;172:395–406. https://doi.org/10.1016/j.ces.2017.06.046.
[18] Helmi A, Voncken RJW, Raijmakers AJ, Roghair I, Gallucci F, van Sint Annaland M. On concentration polarization in fluidized bed membrane reactors. Chem Eng J 2018;332:464–78. https://doi.org/10.1016/J.CEJ.2017.09.045.
[19] Gallucci F, Van Sint AM, Ae A, Kuipers JAM, Van ÁM, Annaland S. Autothermal Reforming of Methane with Integrated CO 2 Capture in a Novel Fluidized Bed Membrane Reactor. Part 2 Comparison of Reactor Configurations Number of CSTRs in the bubble phase N e Number of CSTRs in the emulsion phase. Top Catal 2008;51:146–57. https://doi.org/10.1007/s11244-008-9127-7.
[20] Di Marcoberardino G, Gallucci F, Manzolini G, van Sint Annaland M. Definition of validated membrane reactor model for 5 kW power output CHP system for different natural gas compositions. Int J Hydrogen Energy 2016;41:19141–53. https://doi.org/10.1016/J.IJHYDENE.2016.07.102.
[21] Foresti S, Di Marcoberardino G, Manzolini G, De Nooijer N, Gallucci F, van Sint Annaland M. A comprehensive model of a fluidized bed membrane reactor for small-scale hydrogen production. Chem. Eng. Process. - Process Intensif. 2018;127:136–44. https://doi.org/10.1016/j.cep.2018.01.018.
[22] Di Marcoberardino G, Vitali D, Spinelli F, Binotti M, Manzolini G. Green hydrogen production from raw biogas: a techno-economic investigation of conventional processes using pressure swing adsorption unit. Processes 2018;vol. 6. https://doi.org/10.3390/pr6030019.
[23] Di Marcoberardino G, Foresti S, Binotti M, Manzolini G. Potentiality of a biogas membrane reformer for decentralized hydrogen production. Chem. Eng. Process. - Process Intensif. 2018;129:131–41. https://doi.org/10.1016/j.cep.2018.04.023.
[24] Spallina V, Pandolfo D, Battistella A, Romano MC, Van Sint Annaland M, Gallucci F. Techno-economic assessment of membrane assisted fluidized bed reactors for pure H2 production with CO2 capture. Energy Convers Manag 2016;120:257–73. https://doi.org/10.1016/J.ENCONMAN.2016.04.073.
[25] Brencio C, Maruzzi M, Manzolini G, Gallucci F. Butadiene production in membrane reactors: a techno-economic analysis. Int J Hydrogen Energy 2022;47:21375–90. https://doi.org/10.1016/j.ijhydene.2022.04.259.
[26] Etip bioenergy. Biomethane fact sheet (n.d.), https://www.etipbioenergy.eu/fact-sheets. [Accessed 7 June 2022].
[27] de Nooijer N, Sanchez JD, Melendez J, Fernandez E, Pacheco Tanaka DA, van Sint Annaland M, Gallucci F. Influence of H2S on the hydrogen flux of thin-film PdAgAu membranes. Int J Hydrogen Energy 2020;45:7303–12. https://doi.org/10.1016/j.ijhydene.2019.06.194.

[28] Kato K, Wen CY. Bubble assemblage model for fluidized bed catalytic reactors. Chem Eng Sci 1969;24:1351–69. https://doi.org/10.1016/0009-2509(69)85055-4.
[29] Kunii D, Levenspiel O. Fluidization engineering. 2nd ed. 1991. https://doi.org/10.1016/0032-5910(93)87011-c.
[30] Numaguchi T, Kikuchi K. Intrinsic kinetics and design simulation in a complex reaction network; steam-methane reforming. Chem Eng Sci 1988;43:2295–301. https://doi.org/10.1016/0009-2509(88)87118-5.
[31] Voncken RJW, Roghair I, van Sint Annaland M. A numerical study on concentration polarization in 3D cylindrical fluidized beds with vertically immersed membranes. Chem Eng Sci 2019;205:299–318. https://doi.org/10.1016/j.ces.2019.05.010.
[32] Gas for Climate. Market state and trends in renewable and low-carbon gases in Europe. 2020 14. https://www.europeanbiogas.eu/wp-content/uploads/2020/12/GfC_MSTReport_2020_final.pdf.
[33] 2020 annual CEPCI average value - chemical Engineering | Page 1, (n.d.), https://www.chemengonline.com/2020-annual-cepci-average-value/.